

Gluon Fusion induced Zg and Zgg Productions in the Standard Model at the LHC

Gao Xiangdong and Cai-Dian Lü

*Institute of High Energy Physics and Theoretical Physics Center for Science Facilities,
Chinese Academy of Sciences, Beijing 100049, People's Republic of China*

Qiang Li

*School of Physics, and State Key Laboratory of Nuclear
Physics and Technology, Peking University, China*

(Dated: February 18, 2022)

Abstract

We report calculations of the gluon induced Zg and Zgg productions in the Standard Model at the LHC operating at both 7 TeV and 14 TeV collision energy. We present total cross sections and differential distributions of the processes and compare them with the leading and next-to-leading order QCD $pp \rightarrow Z + 1$ jet, $Z + 2$ jets results. Our results show that the gluon induced Zg and Zgg productions contribute to $pp \rightarrow Z + 1$ jet, $Z + 2$ jets at 1% level.

PACS numbers: 12.38.Bx, 13.85.Qk, 14.70.Hp

I. INTRODUCTION

The CERN Large Hadron Collider(LHC) is acquiring data at a high rate with the center mass energy of 7 TeV, which provides strong experimental support to explore the details of the Standard Model (SM) and investigate new physic (NP). One of the most important relevant processes at the LHC is Z boson production accompanying jets(j) as it is important for both quantitative tests of the SM and serving as backgrounds of NP processes. Thus it is necessary to estimate these processes as more accurate as possible. Z + jets productions at hadron colliders have been extensively studied at QCD leading order(LO) and next-to-leading order(NLO)[1–6] (and references therein).

$gg \rightarrow Zg$ and $gg \rightarrow Zgg$, although formally are finite subsets of the next-to-next-to-leading-order(NNLO) QCD corrections to the processes $pp \rightarrow Zj$ and $pp \rightarrow Zjj$, respectively, can get enhanced at the LHC because of high luminosity of gluon than quarks to compensate the suppression of α_s to some extent. Therefore, it is worthwhile to investigate these processes so as to judge whether their contributions could be ignored or not. In Ref. [7], attention was paid to gluon induced Z boson plus one jet associated production which however shows that the contribution is small as $\sim 1\%$ of the LO result.

In this paper, we update the calculations of $gg \rightarrow Zg$ and report also the results of $gg \rightarrow Zgg$ at the LHC. Comparing them with the LO and NLO Zj and Zjj production rates, we give an estimation of the importance of gluon induced Zg and Zgg productions at the LHC running at both 7 TeV and 14 TeV. This paper is organized as follows. In Sec. II, we give a brief description of our calculations. In Sec. III, we show numerical results and discussions. We close this paper with a summary.

II. DESCRIPTION OF THE CALCULATION

The relevant one-loop Feynman diagrams and amplitudes for the partonic process $gg \rightarrow Zgg$ have been generated with FeynArts 3.6 [8, 9]. The diagrams are sorted into 2 topological classes, corresponding to boxes and pentagons, as shown in Fig. 1. Note that the contributions of triangle diagrams can be neglected [7].

We then use FormCalc 6.2 [13] to manipulate the amplitudes. The Fortran libraries generated with the FormCalc are then linked to our own Monte Carlo integration code

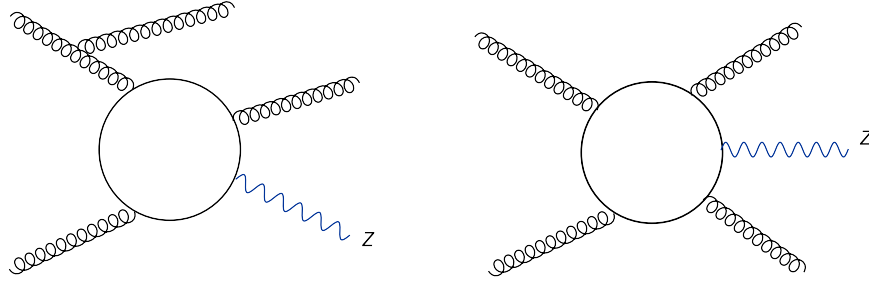


FIG. 1: Feynman Diagrams generated by Jaxodraw [10–12] for the partonic process $gg \rightarrow Zgg$, sorted into 2 topological classes. Taking into account of all possible permutation, one gets 18 diagrams for (a) and 12 ones for (b). In addition, one needs to sum over the Fermion flavors and flow directions within the Fermion loop.

for numerical calculations. The tensor integrals are evaluated with the LoopTools-2.5 [13], which uses the method introduced in Ref. [14] to reduce the pentagon tensor integrals, and Passarino-Veltman procedure [15–18] to reduce lower point ones. The resulting regular scalar integrals are evaluated with the FF package [19, 20]. Moreover, we have implemented the reduction method for pentagon tensor integrals up to rank 5 as proposed in Ref. [21]. We have also implemented in LoopTools the so called alternative Passarino-Veltman reduction for triangle and box tensor integrals [21] to improve numerical stability. We use MCFM [3, 4] to generate results of the $pp \rightarrow Zj, Zjj$ to make a comparison with our results.

We checked the cancelation of ultraviolet and infrared divergences in our calculations, and tested the independence on the mass scale in the Fermion loop. We also checked our results by comparing with numerical results shown in Ref. [7]. We reproduced their results with the same settings and parameters.

III. NUMERICAL RESULTS

In this section we present our numerical results for the total and differential cross sections of the $Z + j$ and $Z + jj$ productions at the LHC. We use CTEQ6L1/CTEQ6M parton distribution functions(PDFs)[22] and default values of corresponding LHAPDF[23] strong coupling α_s for the calculations of the LO/NLO subprocesses. The masses of the W and Z boson and the Fermi constant are taken as input, while the Weinberg angle and the electromagnetic coupling are then calculated using tree level relations of the SM parameters.

Hence, numerically the SM parameters used in our calculations are listed below:

$$\begin{aligned}
 m_W &= 80.398\text{GeV}, \quad m_Z = 91.1876\text{GeV}, \quad G_F = 1.16637^{-5}\text{GeV}^{-2}, \\
 \alpha(m_Z) &= 1/132.3407, \quad \sin^2 \theta_W = 0.22264
 \end{aligned}
 \tag{1}$$

We impose the following cuts to define the jets

$$P_T^j > 40\text{GeV}, \quad |\eta_j| < 4.5, \quad \Delta R_{jj} > 0.6,
 \tag{2}$$

where P_T^j is the transverse momentum of the jets, η_j is the pseudorapidity of the jets and ϕ is the azimuthal angle around the beam direction. ΔR_{jj} define the separation of two jets. Renormalization and factorization scales are set as follows:

$$\mu_r = \mu_f = \mu_0 \equiv \sqrt{P_{TZ}^2 + m_Z^2}.
 \tag{3}$$

Throughout the calculations, six flavors of quark are included in the quark loop with $m_b = 4.6\text{ GeV}$ and $m_t = 173\text{ GeV}$, and all other quarks are taken as massless.

Fig. 2 and Fig. 3 show the renormalization and factorization scales dependences of the total cross sections of gluon fusion induced Zg and Zgg productions and LO $pp \rightarrow Zj, Zjj$ processes at the LHC with $\sqrt{s} = 7\text{ TeV}$ and 14 TeV , respectively. It can be read from Fig. 2 that at the 7 TeV LHC, the total cross section of the gluon induced Zg production varies from 2.1pb to 30.3pb, while Zgg production is from 0.24pb to 9.6pb. Both of the two processes contribute small rates to the Z +jet(s) processes at large scale, however, they counts almost 1% of the total cross sections of the Z +jet(s) productions at small scale ($\sim 0.1\mu_0$), as expected due to larger gluon flux there. At the 14 TeV LHC as in Fig. 3, the total cross sections of the Zg and Zgg productions are around $10 \sim 120\text{ pb}$ and $2 \sim 50\text{ pb}$, which is almost 2% and 1.5% of the total cross sections of the Z +jet(s) productions at small scale ($\sim 0.1\mu_0$). The scale dependence of the gluon induced Zg and Zgg productions in both Fig. 2 and Fig. 3 are larger comparing with LO Z +jet(s) productions for the reason that the loop induced results with higher power of α_s shown here are yet partonic LO.

Fig. 4 and Fig. 5 display the differential distributions of the transverse momentum of the Z boson for the gluon induced Zg and Zgg productions as well as the corresponding LO and NLO Z +jet(s) productions at the LHC with $\sqrt{s} = 14\text{ TeV}$. It can be seen from the two figures that the gluon induced Zg and Zgg productions do not change the shape of the differential distributions of the LO and NLO Z +jet(s) productions, and contribute to the Z +jet(s) productions at a rate similar to that in the total cross sections.

IV. SUMMARY

We have calculated the Zg and Zgg production processes induced by gluon fusion in the framework of the SM at the LHC. Our results show that the total cross sections of the Zg and Zgg productions process at the LHC can be around at $2 \sim 30$ pb with $\sqrt{s} = 7$ TeV and $10 \sim 100$ pb with $\sqrt{s} = 14$ TeV, and $0.2 \sim 10$ pb with $\sqrt{s} = 7$ TeV and $2 \sim 50$ pb with $\sqrt{s} = 14$ TeV, respectively. We also present the differential distributions of the transverse momentum of the Z boson for the two processes. By comparing our results with $pp \rightarrow Zj$ and $pp \rightarrow Zjj$, we conclude that these two channels contribute at an order of $1 \sim 2\%$ to the Zj and Zjj productions at the LHC, at both the total and differential cross section levels.

Acknowledgements

This work is partially supported by National Natural Science Foundation of China under the Grant No. 10735080, and 11075168; Natural Science Foundation of Zhejiang Province of China, Grant No. Y606252 and Scientific Research Fund of Zhejiang Provincial Education Department of China, Grant No. 20051357; and China Postdoctoral Science Foundation under Grant No. 20100480466.

-
- [1] F. A. Berends, W. Giele, H. Kuijf, R. Kleiss, and W. Stirling, Phys.Lett. **B224**, 237 (1989).
 - [2] W. T. Giele, E. W. N. Glover, and D. A. Kosower, Nucl. Phys. **B403**, 633 (1993), hep-ph/9302225.
 - [3] J. M. Campbell and R. Ellis, Phys.Rev. **D65**, 113007 (2002), hep-ph/0202176.
 - [4] J. M. Campbell, R. Ellis, and D. L. Rainwater, Phys.Rev. **D68**, 094021 (2003), hep-ph/0308195.
 - [5] C. F. Berger et al., Phys. Rev. **D82**, 074002 (2010), 1004.1659.
 - [6] H. Ita et al. (2011), 1108.2229.
 - [7] J. van der Bij and E. Glover, Nucl.Phys. **B313**, 237 (1989).
 - [8] J. Kublbeck, M. Bohm, and A. Denner, Comput.Phys.Commun. **60**, 165 (1990).
 - [9] T. Hahn, Comput.Phys.Commun. **140**, 418 (2001), hep-ph/0012260.
 - [10] J. A. M. Vermaseren, Comput. Phys. Commun. **83**, 45 (1994).

- [11] D. Binosi and L. Theussl, *Comput. Phys. Commun.* **161**, 76 (2004), hep-ph/0309015.
- [12] D. Binosi, J. Collins, C. Kaufhold, and L. Theussl, *Comput. Phys. Commun.* **180**, 1709 (2009), 0811.4113.
- [13] T. Hahn and M. Perez-Victoria, *Comput.Phys.Commun.* **118**, 153 (1999), hep-ph/9807565.
- [14] A. Denner and S. Dittmaier, *Nucl.Phys.* **B658**, 175 (2003), hep-ph/0212259.
- [15] G. Passarino and M. Veltman, *Nucl.Phys.* **B160**, 151 (1979).
- [16] M. Consoli, *Nucl.Phys.* **B160**, 208 (1979).
- [17] M. Veltman, *Phys.Lett.* **B91**, 95 (1980).
- [18] M. Green and M. Veltman, *Nucl.Phys.* **B169**, 137 (1980).
- [19] G. van Oldenborgh and J. Vermaseren, *Z.Phys.* **C46**, 425 (1990).
- [20] G. van Oldenborgh, *Comput.Phys.Commun.* **66**, 1 (1991).
- [21] A. Denner and S. Dittmaier, *Nucl. Phys.* **B734**, 62 (2006), hep-ph/0509141.
- [22] J. Pumplin, D. Stump, J. Huston, H. Lai, P. M. Nadolsky, et al., *JHEP* **0207**, 012 (2002), hep-ph/0201195.
- [23] M. Whalley, D. Bourilkov, and R. Group (2005), hep-ph/0508110.

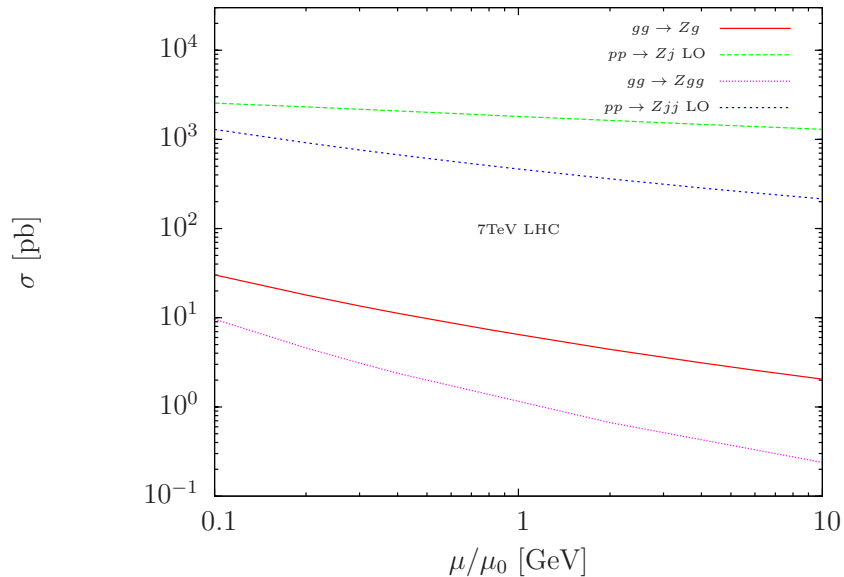


FIG. 2: Scale dependences of the total cross sections for $gg \rightarrow Zg$, Zgg and the LO $pp \rightarrow Zj$, Zjj at the LHC with $\sqrt{s} = 7$ TeV.

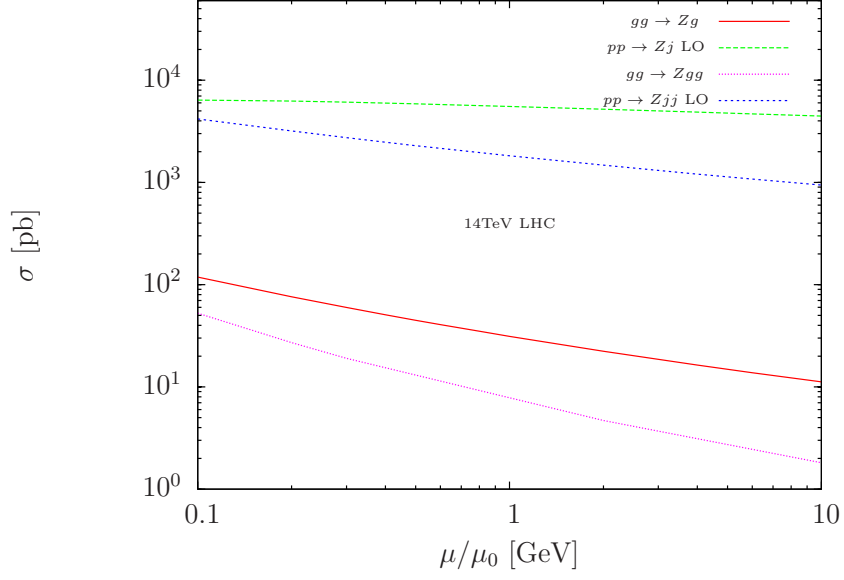


FIG. 3: Scale dependences of the total cross sections for $gg \rightarrow Zg, Zgg$ and the LO $pp \rightarrow Zj, Zjj$ at the LHC with $\sqrt{s} = 14$ TeV.

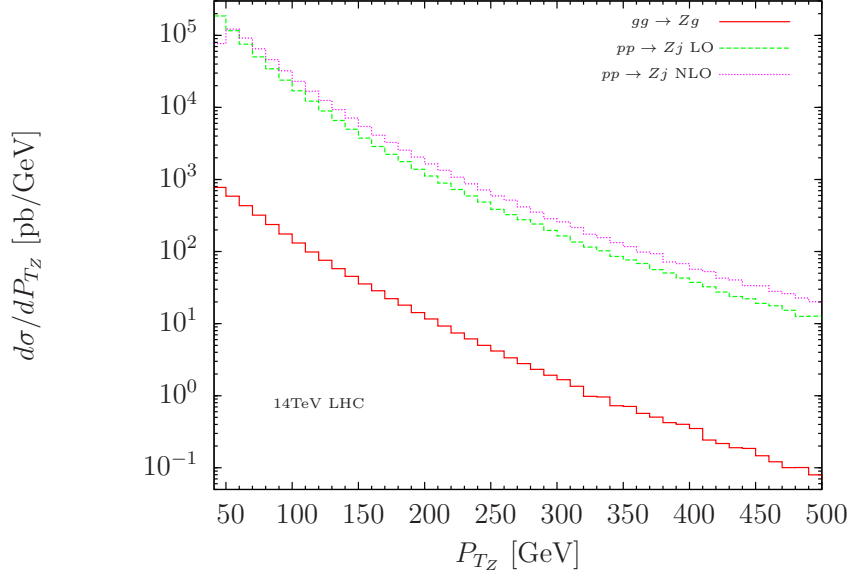


FIG. 4: Differential distributions of the transverse momentum of the Z boson for the process $gg \rightarrow Zg$ and $pp \rightarrow Zj$ at the LHC with $\sqrt{s} = 14$ TeV. The corresponding NLO curves of $pp \rightarrow Zj$ is also plotted with the help of MCFM.

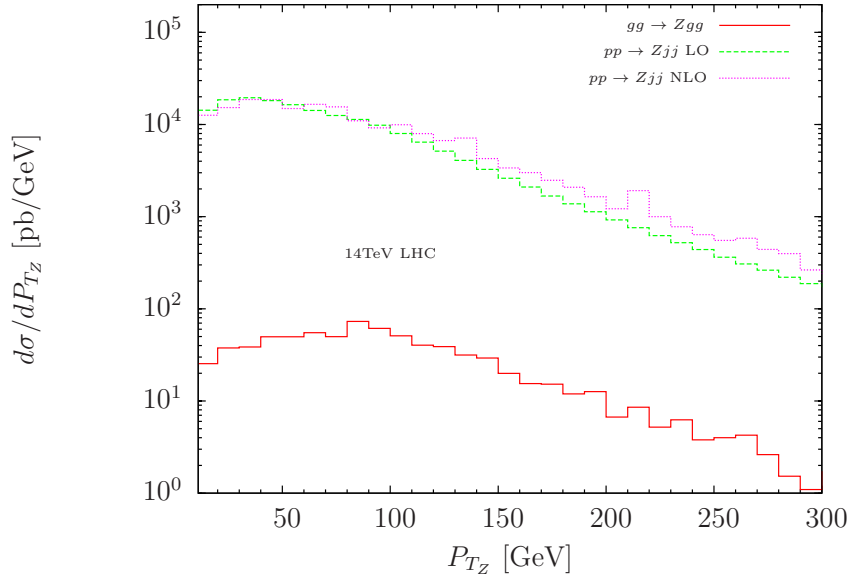


FIG. 5: Differential distributions of the transverse momentum of the Z boson for the process $gg \rightarrow Zgg$ and $pp \rightarrow Zjj$ at the LHC with $\sqrt{s} = 14$ TeV. The corresponding NLO curves of $pp \rightarrow Zjj$ is also plotted with the help of MCFM.